Provided for non-commercial research and education use.
Not for reproduction, distribution or commercial use.

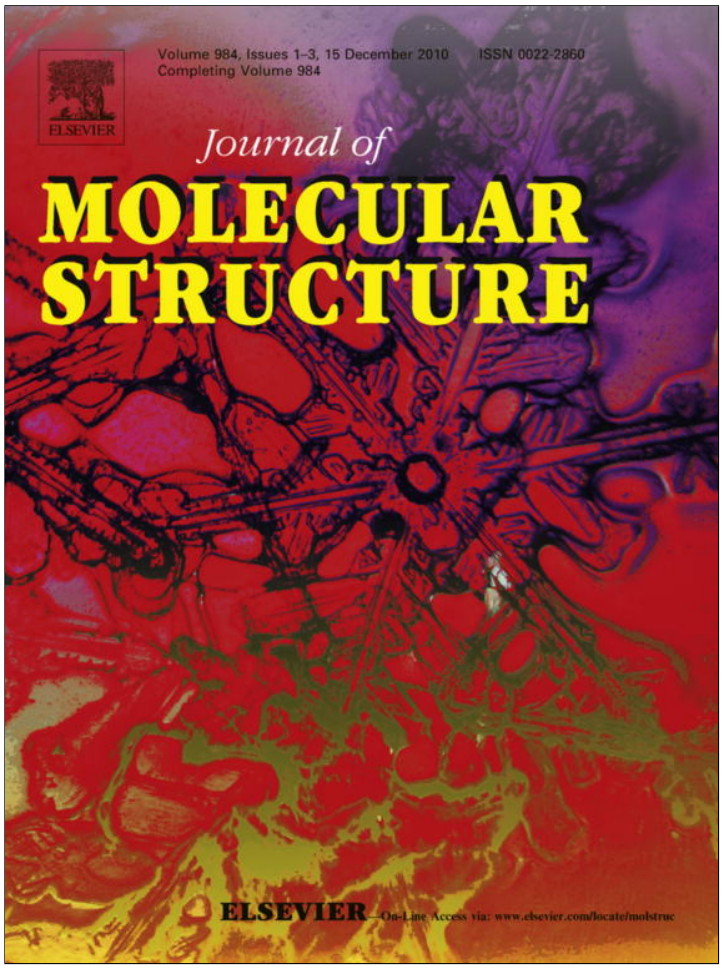

This article appeared in a journal published by Elsevier. The attached copy is furnished to the author for internal non-commercial research and education use, including for instruction at the authors institution and sharing with colleagues.

Other uses, including reproduction and distribution, or selling or licensing copies, or posting to personal, institutional or third party websites are prohibited.

In most cases authors are permitted to post their version of the article (e.g. in Word or Tex form) to their personal website or institutional repository. Authors requiring further information regarding Elsevier's archiving and manuscript policies are encouraged to visit:

http://www.elsevier.com/copyright

Author's personal copy

Journal of Molecular Structure 984 (2010) 300–306

Contents lists available at ScienceDirect

Journal of Molecular Structure

journal homepage: www.elsevier.com/locate/molstruc

Crystal structures and quantitative structure–property relationships of spirobipyrrolidinium and the oxygen-containing derivatives

Seiichiro Higashiya [a,b], Alexander S. Filatov [a], Christopher C. Wells [a], Manisha V. Rane-Fondacaro [b,*], Pradeep Haldar [b]

[a] Department of Chemistry, University at Albany, 1400 Washington Avenue, Albany, NY 12222, USA
[b] College of Nanoscale Science and Engineering, University at Albany, 257 Fuller Road, Albany, NY 12203, USA

ARTICLE INFO

Article history:
Received 25 August 2010
Accepted 29 September 2010
Available online 7 October 2010

Keywords:
Room temperature ionic liquid
Structure–property relationships
Spirobipyrrolidinium
Volume-based thermodynamics
Dielectric constant
Electric double layer capacitor

ABSTRACT

Crystal structures of a popular electrolyte for EDLCs, 1,1′-spirobipyrrolidinium and its oxygen-containing derivatives including $BF_3C_2F_5$ anion are reported. The properties of the BF_4 salts, such as free energy change of fusion and dielectric constants were analyzed using molecular volume information. We used volume-based thermodynamics method to explain the reason for highest melting point in least-polar and most loosely packed crystal. The dielectric constants estimated from volumetric change during the phase changes are consistent with the polarity of the salts. We expect further optimization of these parameters (using known RTILs) to enhance the accuracy of quantitative analysis and prediction.

© 2010 Elsevier B.V. All rights reserved.

1. Introduction

In an earlier publication, we had reported excellent properties of **SBP** $\mathbf{BF_4}$ salt (1,1′-spirobipyrrolidinium (**SBP**, 5-azoniaspiro[4.4]nonane)), and its oxygenated derivatives for electric double layer capacitor applications [1,2]. Their superior chemical and electrochemical robustness, high solubility range, wide voltage window, and conductivity make them especially suitable for electrical energy storage applications, including supercapacitors [3–8]. We have been investigating **SBP**-based oxygen-containing spiroammonium salts for preparation of room temperature ionic liquids (RTILs) without sacrificing other preferable properties [1,2]. Introduction of oxygen atoms to aliphatic ammonium cations frequently lead to formation of low melting point and less viscous salts [9–13] is widely reported.

In this paper, we present the crystal structures of parent **SBP** $\mathbf{BF_4}$ and the oxygen-containing derivatives, 3-oxazolidine-1′-spiropyrrolidinium (**OP**, 2-oxa-5-azoniaspiro[4.4]nonane) $\mathbf{BF_4}$, 3,3′-spirobioxazolidinium (**SBO**, 2,7-dioxa-5-azoniaspiro[4.4]nonane) $\mathbf{BF_4}$, and 2-methyl-3-oxazolidine-1′-spiropyrrolidinium (**2MOP**, 1-methyl-2-oxa-5-azoniaspiro[4.4]nonane) $\mathbf{BF_3C_2F_5}$. In addition, we also discuss the structure–property relationships based on volume-based thermodynamics (VBT) method [14–17] for quantitative evaluation of physicochemical properties of organic onium salts that facilitate further designing of new RTILs with desired properties.

2. Experimental section

2.1. Materials and methods

SBP salt was synthesized by reaction of pyrrolidine and 1,4-dibromobutane; reaction of pyrrolidine, an appropriate aldehyde, and 1-chloro-2-ethanol for **OP** and **2MOP** salts, and reaction of 2-aminoethanol, paraformaldehyde, and 1-chloro-2-ethanol was used for synthesis of **SBO** salt. Reaction of chlorides of **SBP**, **SBO**, and **OP** with $\mathbf{HBF_4}$ led to formation of corresponding $\mathbf{BF_4}$ salts, basically, an ion exchange process [1,2]. $\mathbf{BF_3C_2F_5}$ salt was synthesized using reaction of **2MOP** $\mathbf{BF_4}$ with $\mathbf{KBF_3C_2F_5}$. Repeated recrystallization of **SBP** $\mathbf{BF_4}$ and **SBO** $\mathbf{BF_4}$ salts from isopropanol and water respectively, while **OP** $\mathbf{BF_4}$ and **2MOP** $\mathbf{BF_3C_2F_5}$ were recrystallized from methanol. DSC data were recorded on TA Instruments, DSC 2920 differential scanning calorimeter at 1 atm under dynamic nitrogen flow at a ramp rate of 10 °C min^{-1} in hermetically sealed aluminum pans, and the data was analyzed using TA Instruments universal analysis for Windows95/98NT version 2.6D.

2.2. X-ray crystallography

The X-ray intensity data for all reported complexes were measured on a Bruker SMART APEX CCD X-ray diffractometer system

* Corresponding author. Tel.: +1 518 956 7310; fax: +1 518 437 8687.
E-mail address: mrane@uamail.albany.edu (M.V. Rane-Fondacaro).

0022-2860/$ - see front matter © 2010 Elsevier B.V. All rights reserved.
doi:10.1016/j.molstruc.2010.09.046

Author's personal copy

equipped with a Mo-target X-ray tube (λ = 0.71073 Å) at low temperatures (**SBP BF_4** salt at 100 K, while others at 173 K). In addition, we measured lattice parameters of all salts at 291 K. The frames were integrated with the Bruker SAINT software package [18] using a narrow-frame integration algorithm. The data was corrected for absorption effects using an empirical method (SADABS) [19]. The structures were solved by direct methods and refined using Bruker SHELXTL (Version 6.14) software package [20]. All non-hydrogen atoms were anisotropically refined except for the disordered atoms in **SBP BF_4** compound. In this compound, the cation showed a half-molecule disorder, which was, modeled over two orientations with a 1:1 ratio, while the disorder in **BF_4** anion was modeled over three orientations with 0.5, 0.35, and 0.15 relative occupancies. Hydrogen atoms were independently refined in **SBO BF_4** and **SBP BF_4** using difference Fourier mapping. In **2MOP $BF_3C_2F_5$** all hydrogen atoms were refined independently, except those of a methyl group which were included at idealized positions using a riding model. All hydrogen atoms in the disordered structure of **SBP BF_4** were included at idealized positions for structure factor calculations. Table 1 summarizes selected crystallographic data of all complexes. The CIF files (765950–765953) are freely available upon request from the following web site: www.ccdc.cam.ac.uk/data_request/cif.

2.3. Calculation of free energy change of fusion based on the crystal structures and volume-based thermodynamics

The molecular volumes of salts at 291 K (V_m^{291}) were obtained from the crystal structures. We estimated molecular volumes at a various temperatures $T(V_m^T)$ using volumetric thermal expansion coefficients that were determined from volume change of crystal from low temperature to 291 K. The equations for internal energy (U_{POT} in kJ mol^{-1}) and the standard molar entropy (S°_{298}) of a salt consisting of one cation and one anion are as follows:

$$U_{POT} = 2\left(\frac{\alpha}{\sqrt[3]{V_m}} + \beta\right) \quad (1)$$

$$S^{298} = kV_m + c \quad (2)$$

where α (=117.3 kJ mol^{-1}), β (=51.9 kJ mol^{-1}), κ (=1360 J K^{-1} mol^{-1} nm^{-3}), and c (=15 J K^{-1} mol^{-1}) are the empirical coefficients [14,15]. The heat of lattice formation energy ($\Delta_{latt}H^{298}$) was calculated from U_{POT} for these salts, where, QX consists of a cation Q^{+1} and an anion X^{-1} by adding $2RT$, where R is the gas constant [14,15,21]. $\Delta_{latt}S^{298}$ is the difference between the entropy of the solid salt and the sum of the gas-phase entropies of the individual ions. Eq. (3) gives the standard free energy of ions in lattice ($\Delta_{latt}G^{298}$).

$$\Delta_{latt}G^{298} = \Delta_{latt}H^{298} + T\Delta_{latt}S^{298} \quad (3)$$

We calculated the standard energy change of solvation ($\Delta_{solv}G^{298}$) from the difference in self-consistent field (SCF) energy of the individual ions in vacuum and in dielectric continuum of various dielectric constants using quantum chemical calculations. Quantum chemical calculations were carried out using GAMESS (US) QC package (WinGAMESS09R1) [22] at restricted B3LYP density function, using 6-31 basis set with s diffuse and p polarization functions for hydrogen and sp diffuse and d polarization functions for the other elements (similar to RB3LYP/6-31++G(d,p)) level. Solvation energies in various dielectric constants were calculated with conductor like polarizable continuum model (C-PCM) [23] with $PCM parameters taken from the parameters for hydration (water) by changing the dielectric constant parameter (EPS). The cavity, dispersion, and repulsion energies were not included in free energy change of solvation ($\Delta_{solv}G$) calculation, and only employed the electrostatic interaction. Typical input parameters for the calculation in a dielectric continuum (ε_r = 2) are as follows: $CONTRL SCFTYP = RHF RUNTYP = OPTIMIZE DFTTYP = B3LYP MAXIT = 40 MULT = 1 INTTYP = HONDO ICUT = 11 ITOL = 30 $END $BASIS GBASIS = N31 NGAUSS = 6 NDFUNC = 1 NPFUNC = 1 DIFFSP = .TRUE. DIFFS = .TRUE. $END $SCF DIRSCF = .TRUE. FDIFF = .FALSE. $END $STATPT OPTTOL = 0.0001 NSTEP = 200 HESS = READ HSSEND = .t. $END $FORCE TEMP(1) = 298.15, 377.15, 441.15, 462.15 $END $PCM EPS = 2 EPSINF = 1.7760 VMOL = 18.0700 TCE = 0.00025700 STEN = 71.8100 DSTEN = 0.6500 CMF = 1.2770 RSOLV = 1.3850 ICAV = 0 IDISP = 0 $END.

Finally, the free energy change of fusion ($\Delta_{fus}G$) is calculated from Eq. (4) [15].

Table 1
Crystallographic data and structure refinement for **SBP BF_4**, **OP BF_4**, **SBO BF_4**, and **2MOP $BF_3C_2F_5$** salts.

	SBP BF_4	OP BF_4	SBO BF_4	2MOP $BF_3C_2F_5$
Formula	$C_8H_{16}NBF_4$	$C_7H_{14}NOBF_4$	$C_6H_{12}NO_2BF_4$	$C_{20}H_{32}N_2O_2B_2F_{16}$
FW	213.03	215.00	216.98	658.10
Crystal system	Rhombohedral	Monoclinic	Orthorhombic	Orthorhombic
Space group	*R3c*	$P2_1/n$	$Pna2_1$	*Pbca*
a (Å)	20.791(3)	6.369(4)	12.0719(11)	12.5176(13)
b (Å)	20.791(3)	17.840(10)	6.4498(6)	14.4208(15)
c (Å)	12.561(4)	8.518(5)	11.6510(11)	15.2951(16)
α (°)	90	90	90	90
β (°)	90	101.343(7)	90	90
γ (°)	120	90	90	90
V (Å^3)	4702.0(17)	948.9(10)	907.16(15)	2761.0(5)
Z	18	4	4	4
D_{calcd} (g/cm^{-3})	1.354	1.505	1.589	1.583
Temperature (K)	100(2)	173(2)	173(2)	173(2)
λ (Å)	0.71073	0.71073	0.71073	0.71073
Data/restr/params	917/37/135	2232/0/183	1093/1/175	3163/0/243
Largest diff. peak	0.462	0.495	0.245	0.490
R1[a], *wR2*[b] [$I > 2\sigma(I)$]	0.0984, 0.2725	0.0505, 0.1314	0.0346, 0.0968	0.0664, 0.1773
R1[a], *wR2*[b] (all data)	0.1111, 0.2899	0.0697, 0.1449	0.0372, 0.1000	0.1066, 0.2093
Goodness-of-fit[c]	1.025	1.052	1.121	1.035
CCDC deposition numbers	765950	765952	765951	765953

[a] $R1 = \sum||F_o| - |F_c||/\sum|F_o|$.
[b] $wR2 = [\sum[w(F_o^2 - F_c^2)^2]/\sum[w(F_o^2)^2]]^{1/2}$.
[c] Quality-of-fit $= [\sum[w(F_o^2 - F_c^2)^2]/(N_{obs} - N_{params})]^{1/2}$, based on all data.

Author's personal copy

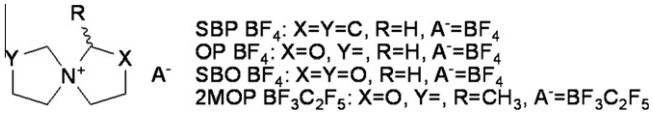

Fig. 1. Various functionalities modifying the parent compound.

$$\Delta_{fus}G = \Delta_{latt}G + \Delta_{solv}G \tag{4}$$

2.4. Estimation of dielectric constant based on the volumetric change during fusion

Enthalpy of each of phase change (glass transition, and fusion) measured by DSC were added, and used as total phase change enthalpy ($\Delta H^{total}_{\mathrm{DCS}}$). Electrostatic ($E^{80}_{elec+pol}$), dispersion ($E_{disp}$), and repulsion interaction (E_{rep}) energies were calculated in a continuum ($\varepsilon_r = 80$) at various cavities, whose size was controlled by scaling factor (ALPHA in $PCMCAV) from 1.0 (van der Waals radii) to 2.0. We obtained the correlation of $E^{80}_{elec+pol}$, E_{disp}, and E_{rep} to the scaling factors, and the cavity volumes from the optimized structures in Section 2.3. Dispersion and repulsion interaction energies were calculated at a Hartree Fock (HF) level owing to the limitation of GAMESS09R1, while the electrostatic interaction energies were calculated using B3LYP DFT. The electrostatic interaction energies in conductor ($\Delta H^{\infty}_{elec+pol}$) was estimated using relationship between $\Delta H^{\infty}_{elec+pol}$, and electrostatic interaction energies in continuum ($\Delta H^{\varepsilon}_{elec+pol}$) with dielectric constant ε_r as follows [23].

$$E^{\varepsilon}_{elec+pol} = (\varepsilon_r - 1)/\varepsilon_r \cdot E^{\infty}_{elec+pol} \tag{5}$$

The total volumetric phase changes (glass transition and fusion) were calculated from the correlations between experimental density (Y) of an ionic liquid, and its calculated density (X) in the solid state for **BF_4^-**, **PF_6^-**, **NTf_2^-**-containing ionic liquids that were reported by Ye et al. [24] as:

$$Y = 0.948X - 0.110 \tag{6}$$

We obtained the volumetric expansion coefficients β_{291} of three **BF_4** salts from the volumetric change of unit cell in the X-ray crystal structures from low temperatures to 291 K. Further, we calculated molecular volume (V^{Tm}_m), and density ($\rho^{Tm,s}$) in the solid state at the melting point; $\rho^{Tm,s}$ was further used to calculate each of the experimental density ($\rho^{Tm,l}$), and thus the molecular volume ($V^{Tm,1}_m$) of an ionic liquid at the melting point.

The molecular volumetric change ($V^{Tm,1}_m - V^{Tm}_m$), the change in internal energy ($\Delta E_{elec+pol} + \Delta E_{disp} + \Delta E_{rep}$) by the molecular volumetric change, and total phase change enthalpy (ΔH_{DCS}) are related as follows:

$$\Delta H_{\mathrm{DCS}} = \Delta E^{\varepsilon}_{elec+pol} + \Delta E_{disp} + \Delta E_{rep} + PN_A(v^{Tm,1}_m - V^{Tm}_m) \tag{7}$$

Thus,

$$\begin{aligned}\Delta E^{\varepsilon}_{elec+pol} &= (\varepsilon_r - 1)/\varepsilon_r \Delta e^{\infty}_{elec+pol} \\ &= \Delta E_{disp} - \Delta E_{rep} - PN_A(V^{Tm,1}_m - V^{Tm}_m)\end{aligned} \tag{8}$$

where P is the atmospheric pressure and N_A is the Avogadro number.

The change in energy for electrostatic, ($\Delta E^{\infty}_{elec+pol}$), dispersion, ($\Delta E_{disp}$) and repulsion ($\Delta E_{rep}$) were obtained from the differences of the energies at the cavity volumes at $V^{Tm,1}_m$ and $V^{T}_m m$ using each of the energy–cavity volume correlations. Finally, we estimated each of the dielectric constants ε_r of the BF_4 salts using these energies and Eq. (8).

3. Results and discussion

3.1. Crystal and molecular structures

The compounds shown in Fig. 1 are crystallized in form of colorless platelets by cooling their respective saturated solutions. The X-ray structural analysis showed rather loose packing of the molecules in crystals with no substantial intermolecular interactions, including those between counter ions. Fig. 2 depicts the cationic parts of the compounds, and Table 1 gives the crystal and structure refinement data.

3.1.1. Pyrrolidine rings

Several papers have reported crystal structures containing **SBP** cations [25–29]. There exist two representative conformations for five-member rings: envelope and twist as shown in Fig. 3.

The quantum chemical calculations resulting from an envelope-envelope (C2-symmetry) conformation of **SBP** rings are more

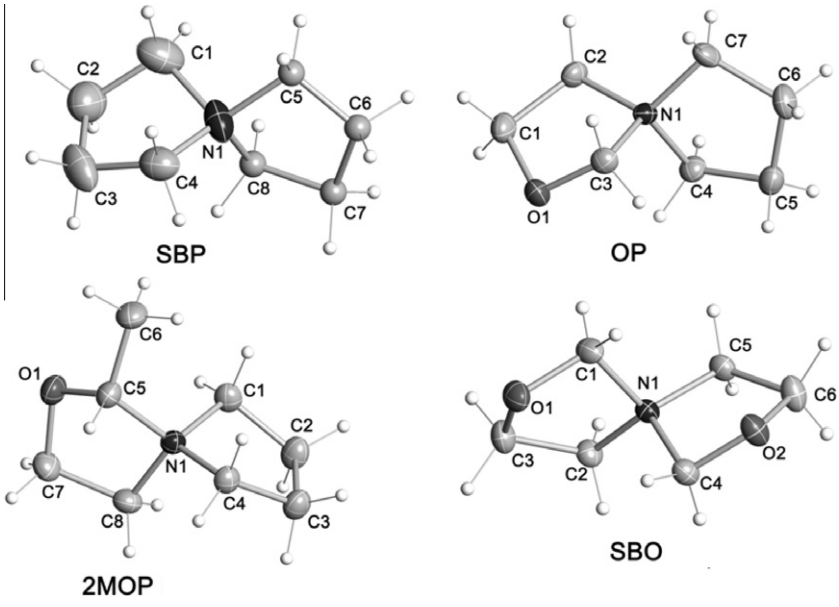

Fig. 2. The cationic fragments of spiroammmonium salts drawn with thermal ellipsoids at the 40% probability levels.

Author's personal copy

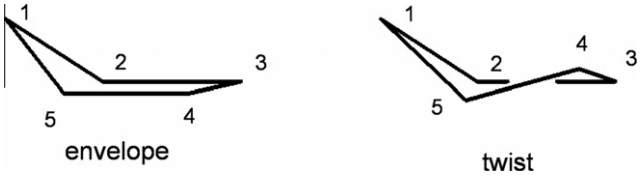

Fig. 3. Two conformations of five-member rings.

stable than a twist-twist (D_2-symmetry) conformation in vacuum by 13 kJ/mol [25–26]. It was attributed the lower symmetry confirmation to packing fraction. Sukizaki et al. concluded that both rings of **SBP BF$_4$** in dimethyl carbonate are in the *N*-flapped envelope confirmations, moreover, the *C*-flapped envelope conformations have slightly lower stability by about 2 kJ/mol [30]. The conformation of **SBP** rings in the crystal structure of **SBP BF$_4$**, which is slightly twisted N-flapped envelope, is consistent with the previous results. In the previously reported crystal structures, the torsion angles created by four carbon atoms of **SBP** rings are the smallest, *i.e.* the nitrogen atoms are located at the most out-of-plane positions in the five-member pyrrolidine rings. Although the *N*-flapped envelope conformations are popular, twisted and *C*-flapped structures have been reported, depending on the crystal packing. In addition, the two pyrrolidine rings in one **SBP** molecule are mostly asymmetric, and **SBP** Br is the only known case possessing the two rings in the same conformation [25,26].

3.1.2. The oxazolidine rings

Simple oxygen-containing spirobipyrrolidinium salts without substitutions has not been reported until recently [1,2]. The torsion angles created by four atoms of oxazolidine rings except for the carbon atoms between the nitrogen and the oxygen atoms are usually the smallest, and thus the conformation of oxazolidine rings are in envelope with flapping the carbon atom between the nitrogen and oxygen atoms. The conformation of SBO is again not symmetrical, one is in C-flapped envelope, and the other is twisted.

3.1.3. Thermal expansion of BF_4 salts

The molecular volume (V_m) observed in oxygen-containing **OP BF$_4$** and **SBO BF$_4$** salts is smaller than in **SBP BF$_4$** salt, and is attributed to large dipole moments and local charges on the cations (Table 2). The unit cell volumes at low temperatures (100 K or 173 K) and 291 K were used to calculate the volumetric thermal expansion coefficients (β_{291}) for each of the BF_4 salts, which was subsequently used to estimate the crystalline molecular volumes at the melting points. **OP BF$_4$** showed the largest β_{291} among three BF_4 salts, followed by **SBO BF$_4$** then followed by **SBP BF$_4$**. Interestingly, the melting point shows the opposite trend.

3.2. Melting point evaluation based on volume-based thermodynamics

The melting points and the crystallographic results led to some intriguing questions. Why the least-polar and most loosely packed **SBP BF$_4$** exhibits the highest melting point among three BF_4 salts, and why **OP BF$_4$** exhibits the lowest melting point. We used volume-based thermodynamics (VBT) method to quantify the physicochemical properties of these salts, and design new RTILs with desired properties. VBT is a simple and powerful method based on the molecular volume to evaluate and predict wide varieties of thermodynamic parameters, and originally designed for inorganic salts.

3.2.1. Free energy change of lattice dissociation $\Delta_{latt}G$

As per VBT, thermal expansion coefficient of salts affects the internal energy (U_{POT}), lattice dissociation enthalpy ($\Delta_{latt}H$), and entropy ($\Delta_{latt}S$). In previous studies, applications of VBT analysis were limited to RTILs whose melting points were closer to room temperature [14–17]. In this study, VBT has been expanded to ammonium salts with higher melting points (>100 °C). In addition, we examined three types of lattice energies corrected with or without thermal expansion. (i) $\Delta_{latt}G^{298,Tm} = \Delta_{latt}H^{291} - T_m\Delta_{latt}S^{291}$ where, both $\Delta_{latt}H^{291}$ and $\Delta_{latt}S^{291}$ were calculated from V_m^{291}. (ii) $\Delta_{latt}G^{Tm} = \Delta_{latt}H^{Tm} - T_m\Delta_{latt}S^{Tm}$ where both $\Delta_{latt}H^{Tm}$ and $\Delta_{latt}S^{Tm}$ were calculated from V_m^{Tm} that was estimated molecular volume at the melting point using volumetric thermal expansion coefficient β_{291} as follows: $V_m^{Tm} = V_m^{291}(1 + \beta_{291}(T_m - 291))$. (iii) $\Delta_{latt}G^{Tm,291} = \Delta_{latt}H^{Tm} - T_m\Delta_{latt}S^{291}$, a combination of $\Delta_{latt}H^{Tm}$ that was calculated from V_m^{Tm} and $\Delta_{latt}S^{291}$ calculated using V_m^{291}. Table 3 summarizes the results of VBT calculations.

3.2.2. Calculation of free energy change of solvation $\Delta_{solv}G$

As the dielectric constants of the salts in this study are unknown, we calculated the solvation energies in continuum using various dielectric constants. Two types of calculation were attempted: (i) solvation free energy change obtained from the difference in SCF total electron energies in vacuum and a certain dielectric continuum ($\Delta_{solv}G^{298}$) [14,15]; (ii) solvation free energy change corrected by thermodynamic parameters calculated at the melting points in a harmonic vibration mode ($\Delta_{solv}G^{Tm}$). Conductor like Polarizable Continuum Model (C-PCM) [23] was used which is similar to COSMO solvation model used in previous reports [14,15].

As expected from the polarity, **SBO BF$_4$** is most stabilized species in the same dielectric continuum, then **OP BF$_4$** and **SBP BF$_4$**. The difference of $\Delta_{solv}G^{Tm}$ from $\Delta_{solv}G^{298}$ (from $\varepsilon_r = 2$ to $\varepsilon_r = 80$) are −9.1 to −6.2 kJ mol^{-1} for **SBP BF$_4$**, −3.2 to −0.25 kJ mol^{-1} for **OP BF$_4$**, and −5.5 to 0.0 kJ mol^{-1} for **SBO BF$_4$** respectively.

3.2.3. Free energy change of fusion $\Delta_{fus}G$ and estimation of dielectric constant

We calculated the free energy change of fusion in dielectric continuums at various dielectric constants by adding various combinations of free energy changes of lattice dissociation and solvation. Representative relationship between $\Delta_{fus}G$ and dielectric constant around the intersection with $\Delta_{fus}G = 0$ is depicted in Fig. 4.

The intersection of each line at $\Delta_{fus}G = 0$ is the predicted dielectric constant. Krossing et al. reported the experimental dielectric constants of various RTILs as 10–15 which well matches with the

Table 2
Selected crystal parameters and lattice energies of BF_4 salts.

	SBP BF$_4$			**OP BF$_4$**			**SBO BF$_4$**		
T_m (°C (K))	189 (462)			104 (377)			168 (441)		
β_{291} (10^{-6} K^{-1})	297			402			373		
T (K)	100	291	T_m	173	291	T_m	173	291	T_m
V_m^T (nm^3)	0.261	0.277	0.291	0.237	0.249	0.258	0.227	0.237	0.250
U_{POT} (kJ mol^{-1})	470.79	463.71	457.81	482.77	476.69	472.49	488.50	482.77	475.96
$\Delta_{latt}H^T$ (kJ mol^{-1})		468.66	465.50		481.64	478.76		487.73	483.30
$\Delta_{latt}S^T$ (kJ mol^{-1} K^{-1})		0.392	0.411		0.354	0.365		0.338	0.356

Author's personal copy

Table 3
Calculated free energy changes of lattice dissociation at various conditions based on VBT.

	T_m (K)	$\Delta_{latt}G^{298}$ (kJ mol^{-1}) ($\Delta_{latt}H^{291} - T_m\Delta_{latt}S^{291}$)	$\Delta_{latt}G^{Tm}$ (kJ mol^{-1}) ($\Delta_{latt}H^{Tm} - T_m\Delta_{latt}S^{Tm}$)	$\Delta_{latt}G^{Tm,291}$ (kJ mol^{-1}) ($\Delta_{latt}H^{Tm} - T_m\Delta_{latt}S^{291}$)
SBP BF$_4$	462	290.38	275.65	284.49
OP BF$_4$	377	376.25	340.95	345.37
SBO BF$_4$	441	387.12	326.39	334.36

values calculated from the intersection at $\Delta_{fus}G = 0$ with correlation of V_m-based correlation term $\Delta_{corr}G$ [14].

We compared the free energy change of fusion $\Delta_{fus}G$, calculated from three methods: (i) summation of $\Delta_{latt}G^{298}$ and $\Delta_{solv}G^{Tm}$ (ii) summation of $\Delta_{latt}G^{Tm}$ and $\Delta_{solv}G^{Tm}$ ($\Delta_{fus}G^{Tm}$) and (iii) summation of $\Delta_{latt}G^{Tm,291}$ and $\Delta_{solv}G^{Tm}$ ($\Delta_{fus}G^{Tm,291,Tm}$). As per those predictions, the dielectric constant of **OP BF$_4$** is greater than that of **SBO BF$_4$** that is counterintuitive to their polarity.

The $\Delta_{fus}G$ and dielectric constants were further corrected by $\Delta_{corr}G$ according to the empirical equation Eq. (9) proposed by Krossing et al. [14]:

$$\Delta_{corr}G = 45\ \text{kJ mol}^{-1}\ \text{nm}^{-3} \cdot V_m\, 5\ \text{kJ mol}^{-1} \tag{9}$$

The calculated correction free energies for V_m^{291} ($\Delta_{corr}G^{291}$), and V_m^{Tm} ($\Delta_{corr}G^{Tm}$) are summarized in Table 4.

After the empirical correction by $\Delta_{corr}G^{291}$, the point of intersection in Fig. 4 moved by 0.3 (**SBP BF$_4$** $\Delta_{fus}G^{Tm}$) to 1.0 (**OP BF$_4$** $\Delta_{fus}G^{298,Tm}$) while the order remained invariant (**SBP** < **SBO** < **OP**). The results are almost identical with $\Delta_{corr}G^{Tm}$. Table 5 summarizes the results of estimated ε_r from the intersections.

The inconsistency in the order of dielectric constants with expected polarity may be partially responsible for insufficient incorporation of polarization term in $\Delta_{latt}G$ in inorganic compound-based VBT.

3.3. Evaluation of dielectric constant derived from density change during the phase changes

Ye and Shreeve reported [24] correlations between the density of various ILs and the relationship between experimental density (Y) for liquid and its calculated density (X) in the solid state as follows:

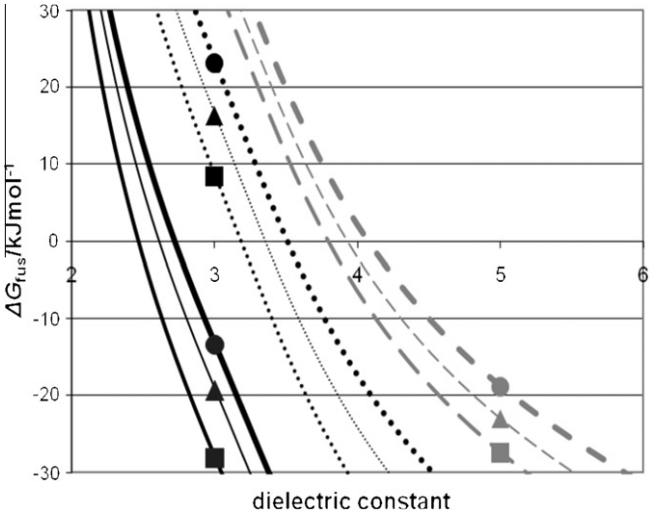

Fig. 4. $\Delta_{fus}G$ at the melting points of salts based on $\Delta_{latt}G^{Tm}$ and $\Delta_{latt}G^{Tm,291}$. Solid lines: **SBP BF$_4$**, gray broken lines: **OP BF$_4$**, dotted lines: **SBO BF$_4$**, thick line with circles: $\Delta_{fus}G^{298,Tm}$; closed squares: $\Delta_{fus}G^{Tm}$; closed triangles: $\Delta_{fus}G^{291,Tm}$.

Table 4
$\Delta_{corr}G$ calculated using V_m^{291} ($\Delta_{corr}G^{291}$) and V_m^{Tm} ($\Delta_{corr}G^{Tm}$).

	$\Delta_{corr}G^{291}$	$\Delta_{corr}G^{Tm}$
SBP BF$_4$	17.46	18.10
OP BF$_4$	16.21	16.59
SBO BF$_4$	15.67	16.27

$$Y = 0.948X - 0.110 (R^2 = 0.998),\quad \text{for } \mathbf{BF_4^-}, \mathbf{PF_6^-}, \mathbf{NTf_2^-}\text{-containing ILs} \tag{10}$$

$$Y = 0.934X - 0.070 (R^2 = 0.999),\quad \mathbf{OTf^-}, \mathbf{CF_3CO_2^-}, \mathbf{N(CN)_2^-}\text{-containing ILs} \tag{11}$$

$$\rho = MW/(602.2\, v_m)\ \text{nm}^3 \tag{12}$$

Gardas and Coutinho further extended this relationship to a wide range of temperatures and pressures [31]. The volumetric difference in experimental liquid density from solid-based calculated density corresponds to the total volumetric change during the phase changes (glass transition and fusion) from crystalline (V_m^{Tm}) to liquid ($V_m^{Tm,l}$) states at the melting point. Furthermore, the total volumetric change during phase changes should have good relation to total enthalpy change of phase changes, which is obtained from DSC. (Our speculation).

Quantum chemical calculations enable one to estimate the changes of electrostatic, dispersion, and repulsion energies due to the change of the volume of molecular cavity. Electrostatic energy depends on both molecular cavity volume and dielectric constant of the continuum in PCM calculation, while dispersion and repulsion energies approximately depend only on the former. Therefore, the total enthalpy of phase change as measured by DSC ($\Delta H_{\text{DCS}}^{total}$) is related to the enthalpy change (internal energy + mechanical work) occurring during volumetric change ($\Delta V_m^{Tm} = V_m^{Tm,l} - V_m^{Tm}$) as follows:

$$\Delta H_{\text{DCS}}^{total} = \Delta E_{elec+pol} + \Delta E_{disp} + \Delta E_{rep} + PN_A(\Delta V_m^{Tm}) \tag{13}$$

where $\Delta E_{elec+pol}$ is energy change of electrostatic and polarization terms, ΔE_{disp} and ΔE_{rep} are the energy changes of dispersion and repulsion terms during the volumetric change from $V_m^{Tm,l}$ to V_m^{Tm}, and P and N_A are pressure and Avogadro constant, respectively. In C-PCM calculation, ΔE_{disp} and ΔE_{rep} depend on the cavity size, while $\Delta E_{elec+pol}$ depend on both the cavity size and dielectric constant. To estimate electrostatic interaction energies at certain dielectric constants, firstly, electrostatic interaction energies in conductor ($\Delta E_{elec+pol}^{\infty}$) should be calculated using relationship between dielectric constant, $\Delta E_{elec+pol}^{\infty}$, and electrostatic interaction energies in continuum with dielectric constant ε_r as shown in Eq. (5) [23].

3.3.1. Total enthalpy change during phase transitions and estimated volumetric change

Table 6 summarizes the calculation results from solid and liquid densities, volumetric change, and mechanical work from volumetric change. We used β_{291} and the original Ye and Shreeve's relationships for the estimation of $V_m^{Tm,l}$ instead of Gardas and Coutinho's expansion.

Author's personal copy

Table 5
Estimation of ε_r from various solvation free energy change $\Delta_{fus}G$.

$\Delta_{fus}G$	$\Delta_{latt}G$	$\Delta_{solv}G$	Salt	ε_r at $\Delta_{fus}G = 0$	ε_r at $\Delta_{fus}G + \Delta_{corr}G^{291} = 0$	ε_r at $\Delta_{fus}G + \Delta_{corr}G^{Tm} = 0$
$\Delta_{fus}G^{298}$	$\Delta_{latt}G^{298}$	$\Delta_{solv}G^{298}$	**SBP BF_4**	4.81		
			OP BF_4	5.76		
			SBO BF_4	5.72		
$\Delta_{fus}G^{298,Tm}$		$\Delta_{solv}G^{Tm}$	**SBP BF_4**	2.74	3.09	3.11
			OP BF_4	4.10	4.84	4.86
			SBO BF_4	3.53	3.95	4.00
$\Delta_{fus}G^{Tm,298}$	$\Delta_{latt}G^{Tm}$	$\Delta_{solv}G^{298}$	**SBP BF_4**	4.78		
			OP BF_4	5.71		
			SBO BF_4	5.68		
$\Delta_{fus}G^{Tm}$		$\Delta_{solv}G^{Tm}$	**SBP BF_4**	2.41	2.75	2.76
			OP BF_4	3.82	4.39	4.43
			SBO BF_4	3.18	3.55	3.55
$\Delta_{fus}G^{Tm,291,298}$	$\Delta_{latt}G^{Tm,291}$	$\Delta_{solv}G^{298}$	**SBP BF_4**	4.80		
			OP BF_4	5.73		
			SBO BF_4	5.70		
$\Delta_{fus}G^{Tm,291,Tm}$		$\Delta_{solv}G^{Tm}$	**SBP BF_4**	2.55	2.96	2.97
			OP BF_4	3.96	4.61	4.63
			SBO BF_4	3.36	3.76	3.76

Table 6
Volume, density, and enthalpy changes at the melting points of salts.

	SBP BF_4	**OP BF_4**	**SBO BF_4**
MW	213.02	215	216.97
V_m^{Tm} (nm^3)	0.291	0.258	0.250
$\rho^{Tm,s}$ ($g\,mL^{-1}$)	1.215	1.386	1.438
$\rho^{Tm,l}$ ($g\,mL^{-1}$)	1.042	1.204	1.254
$V_m^{Tm,l}$ (nm^3)	0.339	0.297	0.287
ΔV_m^{Tm} (nm^3)	0.048	0.039	0.037
$PN_A\Delta V_m^{Tm}$ ($kJ\,mol^{-1}$)	2.95	2.38	2.25

Table 7 provides the DSC measurement data, and total enthalpy change over the phase change. The larger total enthalpy change (ΔH_{DSC}^{total}) reflects the stronger interaction in polar crystals in **SBO BF_4** and **OP BF_4**, as compared with single-phase transition in **SBO BF_4**.

3.3.2. Calculation results of internal energy components by change in cavity volume

Electrostatic ($E_{elec+pol}^{80}$), dispersion (E_{disp}) and repulsion interaction (E_{rep}) energies were calculated in a polar continuum ($\varepsilon_r = 80$) for each of the ions at various cavity sizes were controlled using a scaling factor on van der Waals radii. Addition of each of the energy of a cation and an anion (**BF_4**) at the same scaling factor led to the values of $E_{elec+pol}^{80}$, E_{disp}, and E_{rep} for three salts. From these results, the correlations of $E_{elec+pol}^{80}$, E_{disp}, and E_{rep} to the cavity volumes were fitted using curves in logarithm, exponential, or power, respectively, and the best fitting results were used for further

Table 7
DSC results of spirobipyrrolidinium salt derivatives.

	T_g (°C)	ΔH_g ($kJ\,mol^{-1}$)	ΔS_g /J $K^{-1}mol^{-1}$	ΔH_m ($kJ\,mol^{-1}$)	ΔS_m ($J\,K^{-1}\,mol^{-1}$)	ΔH_{DSC}^{total} ($kJ\,mol^{-1}$)
SBP BF_4	139	3.66	8.38	4.45	9.13	8.12
OP BF_4	64	10.73	29.82	4.38	11.01	15.11
SBO BF_4	–	–	–	24.63	53.07	24.63

Table 8
Relationships between calculated energies and the cavity volume ($\varepsilon_r = 80$).

	Method	Correlation to the cavity volume (x)	R^2	ΔE^{Tm} ($kJ\,mol^{-1}$)	$\Delta E_{elec+pol}^{\infty}$ ($kJ\,mol^{-1}$)
SBP BF_4					
$E_{elec+pol}^{80}$	A	$98.28\ln(x) - 267.09$	0.9844	15.11	15.30
$E_{elec+pol}^{80}$	B	$284.22x^{-0.359}$	0.9997	23.77	24.07
$E_{elec+pol}^{80}$	C	$282.48x^{-0.371}$	0.9998	24.76	25.07
E_{disp}	C	$16.726x^{-1.463}$	0.9998	20.50	
E_{rep}	C	$0.1499x^{-3.806}$	0.9918	−7.29	
OP BF_4					
$E_{elec+pol}^{80}$	A	$-108.7\ln(x) + 264.13$	0.9932	15.31	15.50
$E_{elec+pol}^{80}$	B	$282.16x^{-0.385}$	0.9999	25.10	25.42
$E_{elec+pol}^{80}$	C	$277.63x^{-0.412}$	0.9982	27.37	27.71
E_{disp}	C	$15.812x^{-1.455}$	0.9998	21.08	
E_{rep}	C	$0.1304x^{-3.762}$	0.9931	−13.53	
SBO BF_4					
$E_{elec+pol}^{80}$	A	$-121.3\ln(x) + 255.94$	0.992	16.68	16.89
$E_{elec+pol}^{80}$	B	$280.87x^{-0.407}$	0.999	26.86	27.20
$E_{elec+pol}^{80}$	C	$274.71x^{-0.445}$	0.996	30.19	30.57
E_{disp}	C	$14.849x^{-1.442}$	0.9999	19.66	
E_{rep}	C	$0.1163x^{-3.700}$	0.9944	−7.78	

Method A: calculated at B3LYP-FIXPVA, B: B3LYP-GEPOL-AS, C: HF-GEPOL-AS.

Author's personal copy

Table 9
Estimated electrostatic term from ΔH_{DSC}^{total}, E_{disp}, and E_{rep} and dielectric constants.

Method	$\Delta E_{elec+pol}$ (kJ mol^{-1})	ε_r		
		A	B	C
SBP BF_4	−8.05	0.66	0.75	0.76
OP BF_4	5.19	1.50	1.26	1.23
SBO BF_4	10.49	2.64	1.63	1.52

calculation. In most cases, the power curves yield the best fit. Finally, the energy changes when the cavity volume was changed from V_m^{Tm} to $V_m^{Tm,l}$, and $E_{elec+pol}^{\infty}$ from $E_{elec+pol}^{80}$ according to Eq. (5) were estimated, and the results are summarized in Table 8.

The results from GEPOL-AS ($TESCAV MTHALL = 2) [32] calculation gave better correlation between each of the energy and cavity volume compared with the results from FIXPVA (MTHALL = 4) [33] because the latter method gave significantly smaller cavity volumes. For example, cavity volumes calculated with ALPHA = 1 (van der Waals volumes) using FIXPVA tesseration method gave 48, 52, 54, and 82% smaller than the volume given by GEPOL-AS and other software.

Ionic binding energy consists of Coulombic term (E_{elec}) which is inversely proportional to atomic distance r (thus, $V_m^{-1/3}$ as represented by VBT), polarization term (E_{pol}) has typical distance dependency as r^{-4} (thus $V_m^{-4/3}$), and van der Waals term which is a combination of two terms, repulsion (E_{rep}) and dispersion (E_{disp}) of which typical distance dependency is represented by Lennard–Jones potential as $(\sigma/r)^{12}$–$(\sigma/r)^6$ (thus V_m^{-4} and V_m^{-2}, respectively) [23]. From the calculation results, power orders relative to the cavity volumes are −0.445 to −0.359 for $E_{elec+pol}$; −1.463 to −1.442 for E_{disp}; and −3.806 to −3.700 for E_{rep}, respectively, with smaller than expected orders.

Finally, we calculated $\Delta E_{elec+pol}$ from Eq. (5), the dielectric constant ε_r, obtained according to Eq. (8), and the results summarized in Table 8.

The resulting dielectric constants represent the expected polarity order; however, the values are much smaller (Table 9) than as reported in the literatures [15,34]. The smaller value probably arises due to calculation based on the isolated ions. Optimization of parameters by comparison between calculations of isolated and packed ion pairs [35] will allow precise and crystal structure-independent VBT estimation of the properties such as dielectric constants.

4. Conclusions

We investigated the crystal structures of a widely used electrolyte SBP BF4 and its oxygen-containing derivatives OP BF4, SBO BF4, and 2MOP BF3C2F5. High solubility and conductivity of SBP BF4 in molecular solvents stems from low polarity, and sparsely packed structure. SBP BF4 showed highest melting point among its peers, which is counterintuitive; however, VBT suggests inability of SBP BF4 to acquire sufficient energy from ionic dissolution into its own low dielectric constant liquid state, while SBO BF4 is too polar and densely packed to dissolve. We performed two VBT based calculations to explain the reasons. We attribute the failure of VBT method as reported by Krossing et al. over a wide range of temperature and polarity to missing local polarity, and van der Waals interactions, that are important for large organic molecules. The method based on total volumetric change during phase change estimated the correct order of dielectric constant, while underestimating the value. Parameter optimization calculated from isolated ions by comparison with calculations of packed ion pairs will improve the accuracy of crystal structure-independent VBT estimation of the properties.

Acknowledgements

We are grateful to Dr. John T. Welch of University at Albany for generous support to our project and Dr. Bo Li at University at Albany for X-ray crystallography measurement.

References

[1] S. Higashiya, T.S. Devarajan, M.V. Rane-Fondacaro, C. Dangler, J. Snyder, P. Haldar, Helv. Chim. Acta 92 (2009) 1600.
[2] T. Devarajan, S. Higashiya, C. Dangler, M. Rane-Fondacaro, J. Snyder, P. Haldar, Electrochem. Commun. 11 (2009) 680.
[3] M. Ue, K. Ida, S. Mori, J. Electrochem. Soc. 141 (1994) 2989.
[4] K. Chiba, T. Ueda, H. Yamamoto, Electrochemistry 75 (2007) 664.
[5] K. Chiba, T. Ueda, H. Yamamoto, Electrochemistry 75 (2007) 668.
[6] K. Chiba, Denkai Chikudenki Hyoron (Electrolyt. Condens. Rev.) 57 (2006) 94.
[7] M. Ue, Electrochemistry 75 (2007) 565.
[8] N.M. Jackson, M. Payne, ECS Trans. 16 (2008) 139.
[9] Z.-B. Zhou, H. Matsumoto, K. Tatsumi, Chem. Lett. 33 (2004) 1636.
[10] Z.-B. Zhou, H. Matsumoto, K. Tatsumi, Chem. Lett. 33 (2004) 886.
[11] T. Sato, G. Masuda, K. Takagi, Electrochim. Acta 49 (2004) 3603.
[12] Z.-B. Zhou, H. Matsumoto, K. Tatsumi, Chem. Eur. J. 12 (2006) 2196.
[13] K. Yuyama, G. Masuda, H. Yoshida, T. Sato, J. Power Sources 162 (2006) 1401.
[14] I. Krossing, J.M. Slattery, C. Daguenet, P.J. Dyson, A. Oleinikova, H. Weingaertner, J. Am. Chem. Soc. 129 (2007) 11296.
[15] I. Krossing, J.M. Slattery, C. Daguenet, P.J. Dyson, A. Oleinikova, H. Weingaertner, J. Am. Chem. Soc. 128 (2006) 13427.
[16] L. Glasser, H.D.B. Jenkins, Chem. Soc. Rev. 34 (2005) 866.
[17] L. Glasser, Thermochim. Acta 421 (2004) 87.
[18] SAINT, Version 6.02, Bruker AXS, Inc., Madison, WI, 2001.
[19] SADABS, Bruker AXS, Inc., Madison, WI, 2001.
[20] G. Sheldrick, Acta Crystallogr. A 64 (2008) 112.
[21] H.D.B. Jenkins, J. Chem. Educ. 82 (2005) 950.
[22] W.S. Michael, K.B. Kim, A.B. Jerry, T.E. Steven, S.G. Mark, H.J. Jan, K. Shiro, M. Nikita, A.N. Kiet, S. Shujun, L.W. Theresa, D. Michel, A.M. John Jr., J. Comput. Chem. 14 (1993) 1347.
[23] J. Tomasi, B. Mennucci, R. Cammi, Chem. Rev. 105 (2005) 2999.
[24] C. Ye, J.n.M. Shreeve, J. Phys. Chem. A 111 (2007) 1456.
[25] U.V. Monkowius, SYNTHESE, STRUKTUR UND KOORDINATIONSCHEMIE AUSGEWÄHLTER PHOSPHORORGANISCHER VERBINDUNGEN UND IHRER STICKSTOFF- UND ARSENANALOGA, Anorganisch-chemisches Institut der Technischen Universität München, Technischen Universität München, München, 2004.
[26] U. Monkowius, S. Nogai, H. Schmidbaur, Z. Naturforsch. B 59 (2004) 259.
[27] C.M. Thomas, J.C. Peters, Inorg. Chem. 43 (2004) 8.
[28] J.C. Thomas, J.C. Peters, J. Am. Chem. Soc. 125 (2003) 8870.
[29] S. Sproules, F.I.L. Benedito, E. Bill, T. Weyhermüler, S. DeBeer George, K. Wieghardt, Inorg. Chem. 48 (2009) 10926.
[30] T. Sukizaki, S. Fukuda, T. Yamaguchi, K. Fujii, R. Kanzaki, K. Chiba, H. Yamamoto, Y. Umebayashi, S.-I. Ishiguro, Electrochemistry 75 (2007) 628.
[31] R.L. Gardas, J.A.P. Coutinho, Fluid Phase Equilibr. 263 (2008) 26.
[32] H. Li, J.H. Jensen, J. Comput. Chem. 25 (2004) 1449.
[33] P. Su, H. Li, J. Chem. Phys. 130 (2009) 074109.
[34] C. Wakai, A. Oleinikova, M. Ott, H. Weingaertner, J. Phys. Chem. B 109 (2005) 17028.
[35] M.G.D. Pópolo, C. Pinilla, P. Ballone, J. Chem. Phys. 126 (2007) 144705.